Formation, electrochemical and radical scavenging properties of novel ruthenium compounds with N, X-donor (X = O, N) heterocyclic chelators

Irvin Noel Booysen *, Abimbola Adebisi, Matthew Piers Akerman

School of Chemistry and Physics, University of KwaZulu-Natal, Private Bag X01, Scottsville 3209, Pietermaritzburg, South Africa

ABSTRACT

Herein, we communicate the formation of novel ruthenium compounds with N, X-donor (X = O, N) heterocyclic-derived ligands. A paramagnetic ruthenium(IV) complex, [RuCl(pho)(bzca)(PPh$_3$)](1) (pho = 2-aminophenolate; bzca = 2-carboxylate-1H-benzimidazole) was isolated from the reaction of the ruthenium(II) precursor, trans-[RuCl$_2$(PPh$_3$)$_3$] and 2-((1H-benzimidazole)methylamino)phenol (Hbzap). The 1:1 molar reaction between the same metal precursor and N-(benzoxazole)-2-hydroxybenzamide (H$_2$bhb) led to the formation of cis-Cl, trans-P-[Ru^{III}(Hbhb)Cl$_2$(PPh$_3$)$_2$](2). The dinuclear ruthenium compounds, (μ-Htba,Cl)$_2$[Ru^{II}Cl(PPh$_3$)]$_2$(3) (Htba = N-(thiophene)methyl-benzoxazole-2-amine) and (μ-Cl)$_2$[Ru^{III}Cl(Hchpr)(PPh$_3$)]$_2$(4) (H$_2$chpr = 2-amino-3-((tetrahydro-2H-pyran-4-ylimino)methyl)-4H-chromen-4-one) were formed from the equimolar ratio coordination reactions between trans-[RuCl$_2$(PPh$_3$)$_3$] and the respective free-ligands, Htba and H$_2$chpr. These metal complexes were characterized via IR-, NMR- and UV–Vis spectroscopy, molar conductivity measurements and structural elucidations were confirmed by single crystal X-ray analysis. The X-ray studies revealed that all the metallic compounds exhibited octahedral geometries and that the Hbzap free ligand has undergone a unique molecular transformation to afford the pho and bzca bidentate chelators in 1. The electrochemical properties of the respective metal complexes were investigated by voltammetric analysis. The cyclic voltammograms (CVs) of 1–3 showed one redox couple while within the CV of the dinuclear compound 4, two redox couples were observed. The ligands and their metal complexes were also subjected to DPPH radical scavenging studies. The IC$_{50}$ values showed that all the metallic compounds have higher radical scavenging activities than their corresponding free-ligands and the natural antioxidant, Vitamin C.

© 2015 Elsevier B.V. All rights reserved.

1. Introduction

The concerted efforts in the isolation of new analogues of NAMI A, trans-[RuCl$_4$(DMSO)(Im)](ImH) {ImH = imidazole} are due to its potent anti-metastatic cancer activity [1,2]. Particular interest to us, is the utilization of heterocyclic-derived ligands incorporating benz(imidazole/othiazole/oxazole) moieties due to their multitude of biological activities [3–5]. In addition, the secondary metabolite, chromone and its organic and inorganic compounds have proven to exhibit potent anticancer activities against a wide range of cancer cell lines [6–9]. Most recently, we have also designed Schiff bases containing the tetrahydro-2H-pyrane moiety which shares the same backbone structure as the sugar derivative, mannose. Their structural similarities' can potentially enforce the target specific binding of the tetrahydro-2H-pyrane-derived Schiff bases

and their metal complexes to the mannose receptors in the Sentinel Lymph Node (SLN) [10].

This account details the formation of novel ruthenium compounds containing benzoxazole-amide, benzimidazole-amine and chromone-derived Schiff base ligands. The metal complexes: [RuCl(pho)(bzca)(PPh$_3$)](1) (pho = 2-aminophenolate; bzca = 2-carboxylate-1H-benzimidazole), cis-Cl, trans-P-[Ru^{III}(Hbhb)Cl$_2$(PPh$_3$)$_2$](2), (μ-Htba,Cl)$_2$[Ru^{II}Cl(PPh$_3$)]$_2$(3) and (μ-Cl)$_2$[Ru^{III}Cl(Hchpr)(PPh$_3$)]$_2$(4) were synthesized from the reactions of trans-[RuCl$_2$(PPh$_3$)$_3$] with 2-((1H-benzimidazole)methylamino)phenol (Hbzap), N-(benzoxazole)-2-hydroxybenzamide (H$_2$bhb), N-(thiophene)methyl-benzoxazole-2-amine (Htba) and 2-amino-3-((tetrahydro-2H-pyran-4-ylimino)methyl)-4H-chromen-4-one (H$_2$chpr), respectively. In addition, the redox properties of the metallic compounds 1–4 investigated via voltammetric analysis were comparable to other ruthenium compounds found within the literature [11]. The metallic complexes exhibit higher DPPH radical scavenging activities than their corresponding free-ligands.

* Corresponding author.
E-mail address: Booyseni@ukzn.ac.za (I.N. Booysen).

Hbzap

Htba

H$_2$bhb

H$_2$chpr
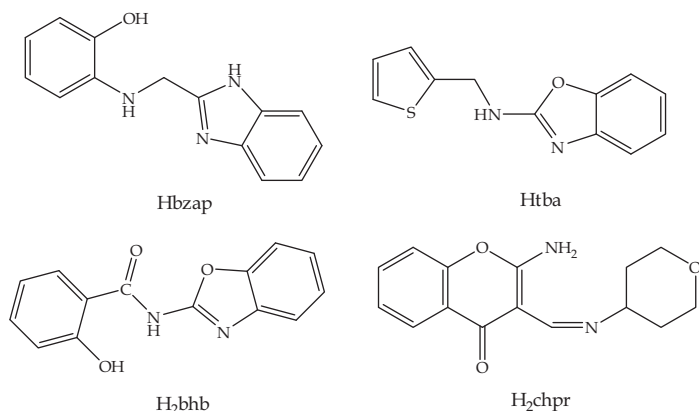
2. Experimental

2.1. Materials and methods

Trans-[RuCl$_2$(PPh$_3$)$_3$], 2-chloromethylbenzimidazole, 2-aminophenol, 2-aminobenzoxazole, salicylaldehyde, 2-thiophene-carboxylde-hyde, 2-amino-3-formylchromone, tetrahydro-2*H*-pyran-4-amine, 2,2-di(4-*tert*-octylphenyl)-1-picrylhydrazyl (DPPH) and electrochemical analysis grade tetrabutylammonium hexafluorophosphate were obtained from Sigma Aldrich. All solvents and common salts were obtained from Merck SA. Reagent grade toluene was dried over sodium wire while the other solvents and chemicals were used without any further purification. Ultrapure water was produced from an Elga Purelab Ultra system.

The infrared spectra were recorded on a Perkin–Elmer Spectrum 100 in the 4000– 350 cm^{-1} range. The ^{1}H NMR spectra was obtained using Bruker Avance 400 MHz spectrometer. All NMR spectra were recorded in DMSO-d_6. UV–Vis spectra were recorded using a Perkin Elmer Lambda 25. The extinction coefficients (ε) are given in dm^3 mol^{-1} cm^{-1}. Melting points were determined using a Stuart SMP3 melting point apparatus. The conductivity measurements were determined at 295 K on a Radiometer R21M127 CDM 230 conductivity and pH meter. Elemental composition of the metallic compounds was determined using a ThermoScientific Flash CHNS/O Analyzer.

Voltammetric measurements were done using an Autolab potentiostat equipped with a three electrode system: a glassy carbon working electrode (GCWE), a pseudo Ag|AgCl reference electrode and an auxiliary Pt counter electrode. The Autolab Nova 1.7 software was utilized for the operation of the potentiostat and data analysis. The ruthenium metal complexes were made up in 2 mM solutions in dichloromethane (DCM) along with tetrabutylammonium hexafluorophosphate (0.1 M) as a supporting electrolyte. Between each measurement, the GCWE electrode surface was polished with a slurry of ultrapure water and alumina on a Buehler felt pad followed by rinsing with excess ultrapure water and ultra-sonication in absolute ethanol.

The experimental procedure of the radical scavenging studies was adapted from a literature method [12]. All experiments were run in triplicate and the percentage radical scavenging activities were determined *via* the following equation:

$$\%\text{Radical scavenging activity} = [(A_c - A_f)/A_c] \times 100$$

where A_c is the absorbance of the control DPPH and A_f is the absorbance upon addition of the ligand or complex to the control, In turn, the IC$_{50}$ values of the respective ligands and their metallic compounds were calculated from the percentage radical scavenging

activity. Firstly, the UV–Vis spectrum of the control (0.2 mM solution of DPPH in DCM) was measured and thereafter 0.1 cm^3 of the metallic compound or the free ligand (30 µM in DCM) were added. The resultant solutions were shaken vigorously, left to stand for 20 min in the dark and then their respective UV–Vis spectra were measured. The Vitamin C analysis was done in a similar manner with the exception that both the Vitamin C solution and its DPPH control solution were prepared in methanol.

2.2. [RuCl(pho)(bzca)(PPh$_3$)](1)

A reaction mixture of Hbzap (0.0250 g; 0.104 mmol) and *trans*-[RuCl$_2$(PPh$_3$)$_3$] (0.1004 g; 0.104 mmol) in toluene (20 cm^3) was heated to reflux under a nitrogen atmosphere for 6 h. A dark brown precipitate was collected *via* filtration, washed with anhydrous diethyl ether and dried under vacuum. This precipitate was recrystallized *via* the slow diffusion of dichloromethane into methanolic solution which yielded XRD quality dark brown crystals. Yield = 55%, M.P. = 250–252 °C. IR (v_{max}/cm^{-1}): v(N–H) 3050, 3025 sh (m), v(O–H) 2552 (w), v(C=O) 1588 (m), v(C=N) 1531, 1514 (vs), v(Ru–PPh$_3$) 693 (vs), v(Ru–O, N)$_{phenolate}$ 466, 430 (s), v(Ru–O, N)$_{benzimidazole}$ 541 (s), 511 (vs). UV–Vis (DMF, (λ_{max} (ε, M^{-1} cm^{-1}))): 232 nm (sh, 31968); 272 nm (sh, 14474); 359 nm (sh, 9806); 435 nm (sh, 6511); 470 nm (5848); 703 (sh, 1977). Conductivity (DCM, 10^{-3} M): 21.94 ohm.cm^{-2} mol^{-1}. *Anal.* Calc. for C$_{33}$H$_{29}$ClN$_3$O$_4$PRu: C, 56.69; H, 4.18; N, 6.01. Found: C, 56.74; H, 4.13; N, 6.16%.

2.3. cis-Cl, trans-P-[Ru(Hbhb)Cl$_2$(PPh$_3$)$_2$](2)

The equimolar amounts of H$_2$bhb (0.0249 g; 0.104 mmol) and *trans*-[RuCl$_2$(PPh$_3$)$_3$] (0.1004 g; 0. 104 mmol) in dichloromethane (20 cm^3) was allowed to stir for 24 h in an open atmosphere. A dark brown solution was obtained after which the volume was reduced and the product was precipitated by addition of *n*-hexane. The complex was recrystallized *via* slow diffusion of dichloromethane into a methanolic solution which resulted in the formation of brown crystals. Yield = 78%, M.P. = 255–257 °C. IR (v_{max}/cm^{-1}): v(O–H) 3051 (w), v(C=N) 1547 (s), v(C–N) 1238 (s), v[Ru–(PPh$_3$)$_2$] 691 (vs), v(Ru–N) 451 (s), v(Ru–O) 433 (m). ^{1}H NMR (295 K/ppm): 7.68–7.52 (m, 30H, 2 x *PPh$_3$*), 7.43–7.38 (m, 4H, *H10, H11, H12, H13*), 7.27–7.21 (m, 4H, *H2, H3, H4, H5*), 5.09 (br, s, 1H, *OH*). ^{31}P NMR (295 K/ppm): 25.38. UV–Vis (DMF, (λ_{max} (ε, M^{-1} cm^{-1}))): 274 nm (sh, 51784); 311 nm (37235); 351 nm (25117); 436 nm (8927). Conductivity (DCM, 10^{-3} M): 26.89 ohm.cm^{-2} mol^{-1}. *Anal.* Calc. for C$_{50}$H$_{39}$Cl$_2$N$_2$O$_3$P$_2$Ru: C, 63.23; H, 4.14; N, 2.95. Found: C, 63.55; H, 4.07; N, 3.22%.

2.4. (μ-Htba,Cl)$_2$[Ru^{II}Cl(PPh$_3$)]$_2$(3)

Compound **3** was isolated from the reaction of Htba (0.0240 g; 0.104 mmol) and *trans*-[RuCl$_2$(PPh$_3$)$_3$] (0.1004 g; 0.104 mmol) in hot benzene (20 cm^3) at reflux under a nitrogen atmosphere for 6 h. The volume was reduced to 5 cm^3 and the product precipitated by the addition of *n*-hexane. Recrystallization of the precipitate was achieved from the slow evaporation dichloromethane:methanol (1:1, *v:v*) solution giving solid dark brown cubic crystals. Yield = 63%, M.P. = 165 –167 °C. IR (v_{max}/cm^{-1}): v(N–H) 3052 (w), v(C=N) 1649 (s), v(thiophene, C=C) 1465, 1436 (s), 1366, 1339 (w), v(C–N) 1246 (m), v(Ru–PPh$_3$) 694 (vs), v(Ru–N)$_{benzimidazole}$ 539 (vs), v(Ru–N)$_{amine}$ 515 (vs). ^{1}H NMR (295 K/ppm): 8.84 (br, s, 2H, *NH, NH′*), 8.53 (t, 2H, *H3, H3′*), 7.84 (t, 2H, *H2, H2′*), 7.68–7.51 (m, 15H, *PPh$_3$*), 7.45–7.32 (m, 15H, *PPh$_3$*), 7.31–7.20 (m, 10H, *Ar, Ar′ Toluene*), 7.15–7.06 (m, 4H, *H1, H1′, H4, H4′*), 7.02–6.96 (m, 6H, *H7, H7′, H8, H8′, H9, H9′*), 4.68 (d, 4H, *H5, H5′, H6, H6′*), 2.08 (s, 6H, *CH$_3$, CH′$_3$* of toluene). ^{31}P NMR (295 K/ppm): 25.55. UV–Vis

(DMF, (λ_{max} (ε, M^{-1} cm^{-1}))): 275 nm (sh, 67628); 404 nm (sh, 14805); 573 nm (9621). Conductivity (DCM, 10^{-3} M): 27.55 ohm.cm^{-2} mol^{-1}. *Anal.* Calc. for C$_{60}$H$_{52}$Cl$_4$N$_6$P$_2$Ru$_2$S$_2$: C, 54.30; H, 3.95; N, 6.33. Found: C, 54.49; H, 3.60; N, 6.57%.

2.5. (μ-Cl)$_2$[Ru^{III}Cl(Hchpr)(PPh$_3$)]$_2$(**4**)

The metal precursor, *trans*-[RuCl$_2$(PPh$_3$)$_3$] (0.1004 g; 0.104 mmol) when reacted with H$_2$chpr (0.0284 g; 0.104 mmol) dissolved in hot anhydrous toluene (20 cm^3) at reflux temperature for 5 h under an open atmosphere, afforded a green mother liquor. From the slow evaporation of this green mother liquor, dark green crystals suitable for X-ray analysis were obtained after several days. Yield = 72%, M.P. = 262–264 °C. IR (ν_{max}/cm^{-1}): ν(N–H) 3053 (w), ν(C=O) 1639 (m), ν(C=N) 1564 (vs), ν(C–O–C)$_{chromone}$ 1437 sh, 1433 (s), ν(C–O–C)$_{tetrahydropyran}$ 1136 (m), ν(Ru–PPh$_3$) 692 (vs), ν(Ru–N)$_{imino}$ 513 (vs), ν(Ru–N)$_{amindo}$ 488 (s). UV–Vis (DMF, (λ_{max} (ε, M^{-1} cm^{-1}))): 257 nm (sh, 28589); 280 nm (sh, 17664); 305 nm (sh, 13147); 355 nm (9632); 465 nm (sh, 4315); 688 nm (sh, 2334). Conductivity (DCM, 10^{-3} M): 22.73 ohm.cm^{-2} mol^{-1}. *Anal.* Calc. for C$_{80}$H$_{76}$Cl$_4$N$_4$O$_6$P$_2$Ru$_2$: C, 60.23; H, 4.80; N, 3.51. Found: C, 60.19; H, 4.78; N, 3.72%.

2.6. X-ray diffraction

Crystal and structure refinement data are given in Table 1. Selected bond lengths and angles are given in Tables 2–4 for **1**, **2** and **4**, respectively. Only a low resolution structure of **3** could be attained. In addition, one disordered toluene molecule was removed from the crystal lattice of compound **4** using Platon Squeeze [13]. In all three cases the data were collected with Mo Kα (λ = 0.71073 Å) radiation at a crystal-to-detector distance of 50 mm. The following conditions were used for data collection: omega and phi scans with exposures taken at 30 W X-ray power and 0.50° frame widths using APEX2 [14]. The data were reduced with the programme SAINT [14] using outlier rejection, scan speed scaling, as well as standard Lorentz and polarization correction factors. A SADABS semi-empirical multi-scan absorption correction [15] was applied to the data. Direct methods, SHELX-2014 [16] and WinGX [17] were used to solve all three structures. All non-hydrogen atoms were located in the difference density map and refined anisotropically with SHELX-2014 [16]. All hydrogen atoms were included as idealised contributors in the least squares process. Their positions were calculated using a standard riding model with C–H$_{aromatic}$ distances of 0.93 Å and U_{iso} = 1.2 U_{eq}, C–H$_{methylene}$ distances of 0.99 Å and U_{iso} = 1.2 U_{eq} and C–H$_{methyl}$ distances of 0.98 Å and U_{iso} = 1.5 U_{eq}. The amine N–H and hydroxyl O–H were located in the difference density map and refined isotropically.

Table 2
Selected bond lengths [Å] and bond angles [°] for **1**.

Ru–O1	2.119(2)
Ru–O2	2.124(2)
Ru–N1	1.904(2)
Ru–N2	2.058(3)
C9–O3	1.225(3)
C9–O2	1.283(4)
O1–Ru–N1	79.5(1)
O2–Ru–N2	76.94(9)

Table 3
Selected bond lengths [Å] and bond angles [°] for **2**.

Ru–P1	2.4229(7)
Ru–P2	2.3979(7)
Ru–Cl1	2.3143(6)
Ru–Cl2	2.3462(6)
Ru–N1	2.120(2)
Ru–O2	2.042(2)
C7–N1	1.321(3)
C7–N2	1.335(3)
C8–N 2	1.343(3)
C8–O2	1.262(2)
C14–O3	1.360(3)
N1–Ru–O2	85.71(7)
Cl1–Ru–Cl2	95.71(2)
P1–Ru–P2	177.38(2)

Table 1
Crystal data and structure refinement data.

	1.CH$_3$CH$_2$OH	**2**	**4**.2(C$_7$H$_8$)
Chemical formula	C$_{33}$H$_{29}$ClN$_3$O$_4$PRu	C$_{50}$H$_{39}$Cl$_2$N$_2$O$_3$P$_2$Ru	C$_{80}$H$_{76}$Cl$_4$N$_4$O$_6$P$_2$Ru$_2$
Formula weight	699.08	949.74	1595.33
T (K)	100(2)	296(2)	100(2)
Crystal system	Monoclinic	Triclinic	Triclinic
Space group	P2$_1$/n	P$\bar{1}$	P$\bar{1}$
Unit cell dimensions			
a (Å)	12.5002(6)	12.8703(7)	12.8091(5)
b (Å)	19.6974(8)	12.8876(7)	12.9652(6)
c (Å)	12.6428(5)	14.8744(8)	13.7695(6)
α (°)	90	85.899(2)	68.311(2)
β (°)	107.511(2)	70.720(2)	76.094(2)
γ (°)	90	65.173(2)	82.489(2)
V (Å^3)	2968.7(2)	2107.1(2)	2060.34(15)
Z	4	2	1
D_{calc} (Mg/m^3)	1.564	1.497	1.286
Absorption coefficient (mm^{-1})	0.716	0.622	0.585
$F(000)$	1424	970	818
θ range for data collection (°)	1.98; 26.03	1.75; 26.16	1.63; 26.11
Reflections measured	16731	35691	33857
Observed reflections [$I > 2\sigma(I)$]	5837	8256	7981
Independent reflections	4698	7043	7260
Data/restraints/parameters	4698/0/401	7043/1/545	7260/0/447
Goodness of fit (GOF) on F^2	1.028	1.026	1.045
Observed R, wR^2	0.0363, 0.0767	0.0280, 0.0603	0.0282, 0.0726
R_{int}	0.040	0.034	0.22
$\Delta\rho_{max}$, $\Delta\rho_{min}$ (e Å^{-3})	0.57, −0.47	0.43, −0.37	0.95, −0.33

Table 4
Selected bond lengths [Å] and bond angles [°] for **4**.

Ru–Cl$_{terminal}$	2.3744(7)
Ru1–Cl1	2.4967(5)
Ru2–Cl2	2.4967(5)
Ru1–Cl2	2.4283(6)
Ru2–Cl1	2.4283(6)
Ru–P	2.3315(5)
Ru–N$_{Schiff\ base}$	2.026(2)
Ru–N$_{amido}$	1.972(2)
Cl1–Ru1–Cl2	84.94(2)
Cl1–Ru1–Cl3	89.73(2)
N2–Ru1–N1	87.93(7)
P1–Ru1–Cl2	178.75(2)
N2–Ru1–Cl1	170.77(5)
N1–Ru1–Cl3	175.55(5)

3. Results and discussion

3.1. Synthesis and spectral characterization

The respective free-ligands were attained in good yields and spectroscopic characterization provided definitive insight into their individual molecular structures, see Figs. S1–S8. The metallic compounds exhibit remarkably good solubility in all chlorinated solvents and selected high boiling point aprotic solvents including dimethylformamide and dimethylsulfoxide but poor solubility in alcoholic media. The low molar conductivity values of the metallic compounds **1**–**4** are testimony to their electrical neutrality and these values were similar to other neutral ruthenium(II), -(III) and -(IV) compounds found within the literature [11,18].

A proposed route to the formation of **1** is illustrated in Scheme 1. The first step entails the equimolar ratio reaction between the metal precursor and ligand, Hbzap which afforded the ruthenium(II) intermediate, [RuCl(bzap)L$_2$] (L = PPh$_3$). Despite
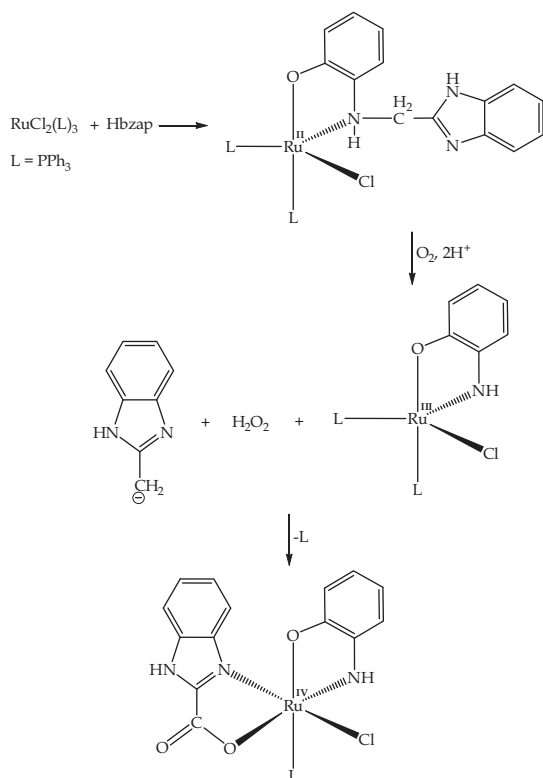
Scheme 1. Proposed formation route of [RuCl(pho)(bzca)(PPh$_3$)](**1**).

the use of an inert nitrogen atmosphere, dimolecular oxygen diffused into the refluxing toluene solution. In turn, the dimolecular oxygen in the presence of H$^+$ ions and the ruthenium(II) intermediate afforded molecular hydrogen peroxide in the reaction mixture. This is supported by the patent of Diamond et al., who's study has shown that hydrogen peroxide can be generated by the oxidation of their formulated ruthenium(II) compounds to analogous ruthenium(III) compounds in the presence of dimolecular oxygen and H$^+$ ions [19]. This is followed by instantaneous C–N amine bond cleavage induced by hydrogen peroxide [20]. The residual hydrogen peroxide acts as a co-catalyst with the ruthenium(III) intermediate, [RuCl(pho)L$_2$] which oxidizes the 2-methyl-1*H*-benzimidazole carbo-anion to 2-carboxylate-1*H*-benzimidazole (bzca) [21,22]. Then the bzca moiety then coordinates to the ruthenium and the residual hydrogen peroxide oxidizes the metal centre to its + IV oxidation state. This ultimately led to the paramagnetic ruthenium(IV) centre of **1** being surrounded by the two bidentate chelators (*viz.* monoanionic bzca and dianionic pho), see Fig. 2.

The Hbhb chelator of complex **2** acts as monoanionic bidentate chelator through the amide oxygen (O2) and benzoxazole nitrogen (N1), see Fig. 3. Furthermore, this mononuclear ruthenium complex **2** is stabilized by the *trans*-[Ru(PPh$_3$)$_2$] core. The metal centres of the dinuclear compounds **3** and **4** are bridged by chloro ligands while the former is reinforced by the bidentate coordination of the neutral Htba chelators through the benzimidazole and amine nitrogens to the respective metal centres, see Figs. 4 and S9. For compound **4**, each monoanionic Hchpr chelator coordinates in a bidentate manner through their singly deprotonated amino groups and neutral imino nitrogens. Furthermore, the octahedral coordination spheres for each metal centre in **3** and **4** are completed by mono-triphenylphosphine and chloro co-ligands.

Mutual intense stretches are observed in the IR spectra of all the metallic compounds [at 693 cm^{-1} (for **1**), 691 cm^{-1} (for **2**), 694 cm^{-1} (for **3**) and 692 cm^{-1} (for **4**)] ascribed to the v(Ru–PPh$_3$) vibrations, see Figs. S5–S8. In addition, in the IR spectra of the respective metallic compounds, distinctive low intensity vibrations are also found below 600 cm^{-1} due the Ru–N and Ru–O coordination bonds. The absence of the C–N stretch (at 1277 cm^{-1} for Hbzap) in the IR spectrum of **1** indicated that the Hbzap ligand has cleaved into bzca and pho moieties. Furthermore, the coordination of the bzca moiety is affirmed by the v(C=N) vibration appearing as two splitted stretches compared to that of the free-ligand which is found at 1513 cm^{-1} as a broad single vibrational band. For complex **2**, the heterocyclic C=N vibrational band appears at a lower frequency (at 1547 cm^{-1}) in comparison to the corresponding vibrational band of its free ligand occurring at 1601 cm^{-1}. Similarly for the dinuclear ruthenium compound **4**, evidence of coordination of its chelators, is given by the C=N vibrational band of **4** shifting to lower frequencies [1546 cm^{-1} for **4** and 1601 cm^{-1} for H$_2$chpr]. For complex **3**, the C–N amine vibration is at a common frequency (at 1246 cm^{-1}) with respect to the analogous band of its free ligand, Htba.

Proof of chelation can also be attained from NMR spectral analysis of the diamagnetic compound **3**. The Htba ligands exhibit magnetic equivalence given by the fact that the signals resonate at the same position and that each signal integrates to double to that what is expected for one Htba chelator, see Fig. S10. For example, a broad singlet is observed at 8.84 ppm for the amine protons (for *NH* and *NH'*) whereas for the free-ligand, Htba a broad singlet integrating to one is found at 8.50 ppm for the amine proton. For **3**, the signals of the respective triphenylphosphine co-ligands does not coalesce but rather appear as two intense multiplets each integrating to 15 protons. Despite the trend observed with respect to the triphenylphosphine co-ligands in the proton NMR spectrum of **3**, the phosphorous signals of **3** (at 25.55 ppm) appear as a single peak indicating magnetic equivalence.
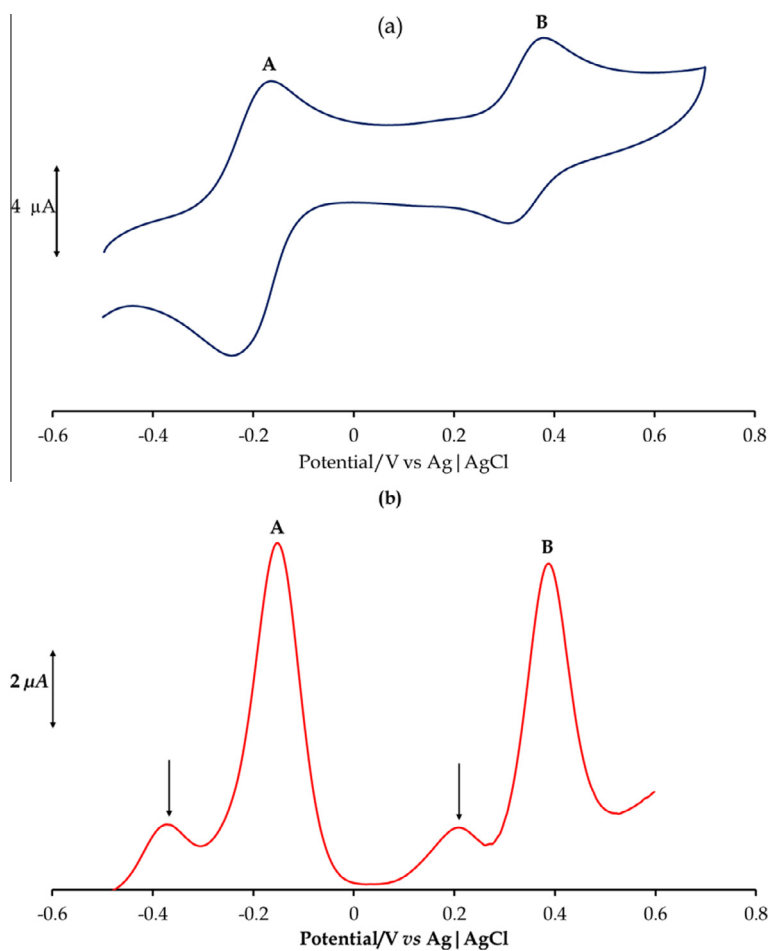
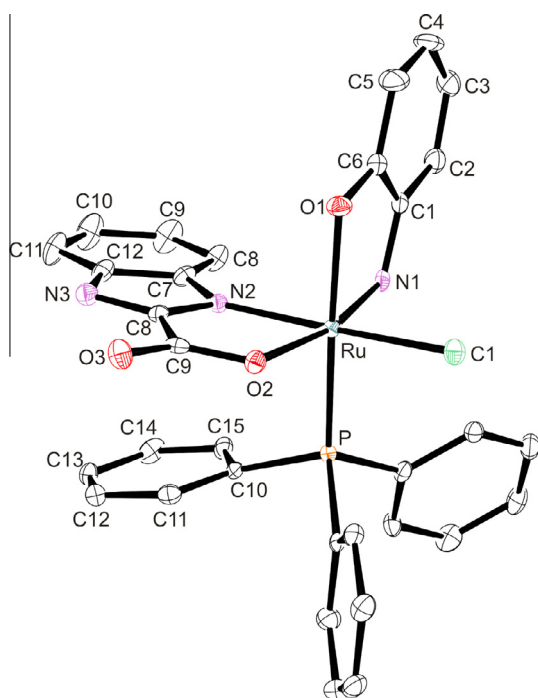Fig. 1. (a) CV and (b) SWV of compound **4** at 100 mV/s.

Fig. 2. An ORTEP view of complex **1** showing 50% probability displacement ellipsoids and the atom labelling. The hydrogen atoms and ethanol molecule of recrystallization were omitted for clarity.
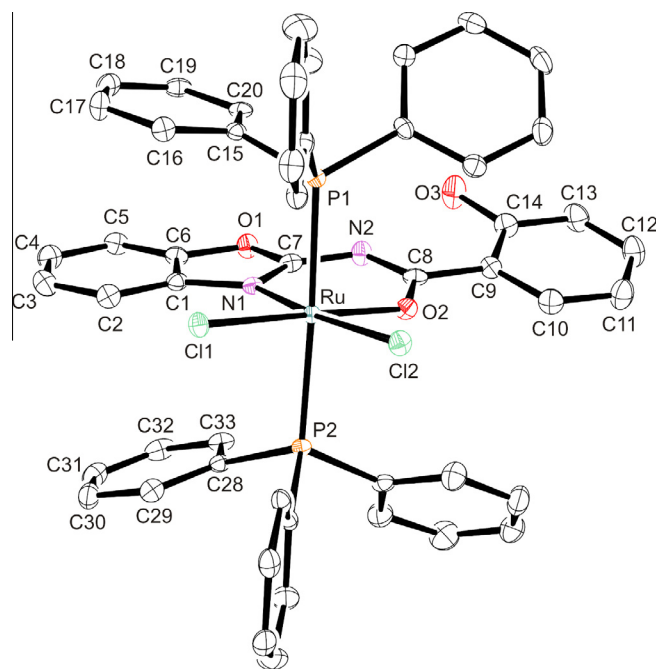
Fig. 3. An ORTEP view of complex **2** showing 50% probability displacement ellipsoids and the atom labelling. The hydrogen atoms were omitted for clarity.
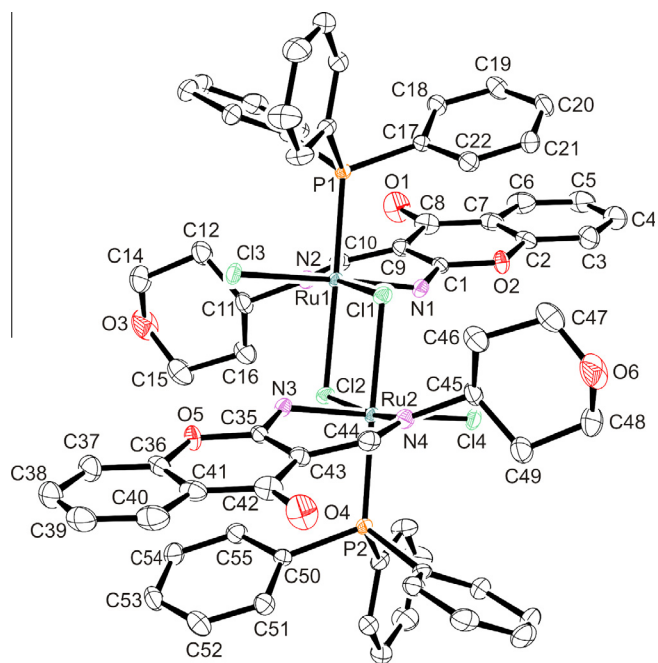
Fig. 4. An ORTEP view of compound **4** showing 50% probability displacement ellipsoids and the atom labelling. The hydrogen atoms and toluene solvent molecules of recrystallization were omitted for clarity.

Several common $\pi-\pi^*$ intraligand transitions are observed below 400 nm in the overlay UV–Vis spectra of the free ligands and their metallic compounds **1–4**, see Figs. S11–S14. In addition, at red-shifted wavelengths between 400 and 600 nm, Ligand-to-Metal-Charge-Transfer (LCMT) bands are found. As expected the low spin d^6 metallic compound **3** has no metal-based electronic transitions while for the paramagnetic ruthenium(III) compounds **1** and **4**: a distinctive $d-d$ transition for compound **4** (at 688 nm) and a shoulder with a low extinction coefficient for complex **1** (at 703 nm) is observed. However, for the d^5 complex **2**, no $d-d$ transition was observed which could be due to a higher band-gap energy and thus the metal-based electronic transition is unfavourable.

3.2. Electrochemistry studies

The cyclic voltammograms (CVs) of **1–3** showed one redox couple while within the CV of the dinuclear compound **4**, two redox couples labelled **A** and **B** can be found, Fig. 1, S15 and S16. All the redox couples exhibits diffusion controlled behaviour at increasing scan rates, see Fig. S17 for the overlay CVs of compound **4** at incrementing scan rates. Furthermore, the redox couples corresponds to one electron redox processes indicated by their respective peak current ratios (I_{pa}/I_{pc}) which approach one. In addition, all these metallic compounds exhibit quasi-reversible behaviour indicated by their peak to peak separations which are different to the standard, ferrocene (90 mV at 100 mV/s), refer to Table 5. More

Table 5
Electrochemical parameters of the respective metallic compounds at 100 mV/s.

Compound	1	2	3	4	
				A	B
E_{pa}/V	0.025	−0.063	0.471	−0.241	0.384
E_{pc}/V	0.120	−0.146	0.280	−0.163	0.313
$E_{1/2}$/V	0.073	−0.105	0.376	−0.202	0.349
ΔE/mV	95	83	191	78	71

specifically, the redox couples of the metallic compounds **1–3** exhibit slower electron transfer kinetics compared to compound **4**'s redox couples **A** and **B**. The halfwave potential of complex **1** is assigned to the Ru(III/IV) redox couple as it was found at a slightly lower potential than the paramagnetic diamido ruthenium(IV) complex, *trans-P*, *cis-Cl*-[RuCl₂(ddd)(PPh₃)₂] (H₂ddd = 5, 6-di-amino-1,3-dimethyluracil) [11]. For compounds **2** and **3**, their half-wave potentials are ascribed to the Ru(II/III) redox couple as they have comparable redox behaviour as other ruthenium compounds reported in the literature [11,19]. Similarly, the dinuclear ruthenium(III) compound **4** had analogous redox behaviour (redox couples **A** and **B** assigned to the Ru(II/III) and Ru(III/IV) process, respectively) as the paramagnetic ruthenium(III) complex, [RuCl(bsp)₂(PPh₃)] {Hbsp = *N*-(2-hydroxybenzylidene)-benzothiazole} [23]. Noticeably, using the more sensitive square wave voltammetry technique, at lower potentials relative to each redox process (*viz.* **A** and **B**), two smaller peaks are observed, see Fig 1(b). These peaks indicated by the arrows are due to the second metal centre undergoing analogous redox processes.

3.3. Radical scavenging studies

An increase of radicals within the human body can have detrimental effects on human health by inducing numerous diseases like cancer, arthritis, Parkinson's or Alzheimer's diseases [24–26]. Thus, there is an upsurge in research to discover novel antioxidants which may offer higher radical scavenging capabilities than common natural antioxidants, *e.g.* vitamin C. Transition metal complexes with redox active metal centres have shown to exhibit optimal radical scavenging capabilities for a wide range of radicals by donating an electron to quench the radical specie [27,28]. Alternatively, transition metal complexes with aromatic hydrocarbon ligands can also act as proton donors to neutralize radicals [29]. In our study, the formulated metallic compounds **1–4** were subjected to DPPH radical scavenging activities. The IC₅₀ values showed that all the metallic compounds [89.98 μM (for **1**), 61.50 μM (for **2**), 96.40 μM (for **3**) and 66.31 μM (for **4**)] have higher radical scavenging activities than their corresponding free-ligands [112.53 μM (for Hbzap), 87.87 μM (for H₂bhb), negligible (for Htba) and 300 μM (for H₂chpr)]. Despite the negligible radical scavenging activity of the free ligand, Htba, the presence of the two metal centres in compound **3** induced an optimal activity. In fact, the unpaired *d*-electron configurations of the ruthenium(III) metal centres promoted the highest DPPH radical scavenging activity judged by its lower IC₅₀ value. Furthermore, all the metallic compounds had considerable higher radical scavenging capabilities that the natural antioxidant, vitamin C (IC₅₀ value = 147 μM). The observations are well in agreement with other ruthenium(II) and –(III) compounds found within the literature [30–32].

3.4. Crystal structure of [RuCl(pho)(bzca)(PPh₃)](**1**)

Complex **1** exhibits a distorted octahedral geometry which is imposed on by the O1–Ru–N1 (79.5(1)°) and O2–Ru–N2 (76.94(9)°) bite angles which is significantly narrower than the ideal octahedral angle of 90°. Furthermore, the crystal lattice is stabilized by $\pi-\pi$ stacking (interplanar spacing of 3.405 Å) between the nearly co-planar C10–C15 phenyl group and the imidazole ring of the bzca chelator. In addition, re-enforcement is given by classical intermolecular (Cl···H26–O4 = 2.40(5) Å) (O4···H25A-N3A = 1.91(4) Å and O3···H24B–N1B = 2.09(3) Å) hydrogen bonding. Ultimately, these molecular interactions lead to columns of **1** running parallel to the [*b*]-axis, refer to Fig. S18 and Table S1.

In contrast to the nearly equidistant Ru–O bonds (Ru–O1 = 2.119(2) Å and Ru–O2 = 2.124(2) Å), the ruthenium to

monoanionic amido nitrogen bond (Ru–N1 = 1.904(2) Å) and neutral benzimidazole (Ru–N2 = 2.058(3) Å) nitrogen bond differs as expected. In addition, the Ru–N1 coordination sphere bond length is comparable to the analogous amido bonds of the paramagnetic ruthenium(IV) complex, *trans-P*, *cis-Cl*-[RuCl$_2$(ddd)(PPh$_3$)$_2$] [11]. The carboxylate form of the bzca chelator is confirmed based on the C–O bond orders which can be readily distinguished by their respective bond distances (C9–O3 = 1.225(3) Å and C9–O2 = 1.283(4) Å).

3.5. Crystal structure of cis-Cl, trans-P-[Ru^{II}(Hbhb)Cl$_2$(PPh$_3$)$_2$](2)

The molecular structure of **2** crystallizes out in a $P\bar{1}$) space group with two molecules occupying the triclinic unit cell. The bidentate coordination of the Hbhb chelator results in the formation of a constrained N1–Ru–O2 bite angle [85.71(7)°] which pushes the chloro co-ligands (Cl1–Ru–Cl2 = 95.71(2)°) more further apart from the ideal octahedral angle of 90°. Furthermore, the influence of cyclometallation is clearly evident from the deviation from linearity of the *trans*-[Ru(PPh$_3$)$_2$] core (P1–Ru–P2 = 177.38(2)°) and variable Ru–P bond lengths (Ru–P1 = 2.4229(7) Å and Ru–P2 = 2.3979(7) Å). Indicative to complex **1**, complex **2** has a series of intermolecular interactions. Hydrogen bonding interaction exists between the phenolic hydrogen and amide nitrogen atoms (O3–H39⋯N2 = 1.74(3) Å). This interaction is accompanied by interactions of the C1–C6 phenyl ring with the C15–C20 (3.598 Å) and C28–C33 (3.742 Å) phenyl rings. Subsequently, this leads to the benzoxazole moiety affording a dihedral angle of 17.58° with respect to the phenolic moiety and the molecules of **1** stacking in columns parallel to the [*b*]-axis, see Fig. S19.

The *cis*-Ru–Cl coordination bonds (Ru–Cl1 = 2.3143(6) Å and Ru–Cl2 = 2.3462(6) Å) are different due to the difference in the *trans*-influences of the ketonic O2 and N1 benzoxazole atoms. However, these distances are shorter than the ruthenium halide bond of **1** which is ascribed to the higher Lewis acid character of the metal centre of **1**. Interestingly, within the cyclometallated RuN1C7N2C8O2 ring, the deprotonation of the amide nitrogen resulted in a delocalized *pi*-conjugated system throughout the N1C7N2C8O2 moiety which can evidently be affirmed by the comparable C7–N1 (1.321(3) Å), C7–N2 (1.335(3) Å) and C8–N2 (1.343(3) Å) bond distances and the significant difference between the bond distances of C8–O2 (1.262(2) Å) from C14–O3 (1.360(3) Å).

The literature shows that numerous ruthenium benz(oxazole/imidazole) complexes with diverse structural features have been isolated. Among these complexes, is the mononuclear ruthenium(II) complex, *trans*-[RuCl$_2$(Hbo)(PPh$_3$)$_2$] (Hbo = 2-hydroxyphenylbenzoxazole) which has an identical Ru–N$_{benzoxazole}$ (2.120(2) Å) bond length as complex **2** (Ru–N1 = 2.120(2) Å) [33]. The Ru–N$_{benzimidazole}$ (2.058(3) Å) of complex **1** is comparable to the paramagnetic complex, *trans*-[Ru^{III}Cl(bzp)(PPh$_3$)$_2$] (Hbzp = *N*-(2-hydroxybenzylidene)benzimidazole) (Ru–N$_{benzimidazole}$ = 2.069(4) Å) [23]. Furthermore, as expected the Ru–O2 (2.124(2) Å) bond distance of **1** is shorter than the analogous bond distances of the ruthenium(II) complex, *cis*-[Ru(bzca)$_2$(PPh$_3$)$_2$] (Ru–O$_{carboxylate}$ = 2.133(4) Å and 2.117(4) Å) [34].

3.6. Crystal structure of (μ-Cl)$_2$[RuCl(Hchpr)(PPh$_3$)]$_2$(4)

Each molecule of **4** crystallizes out in a $P\bar{1}$) space group along with two toluene molecules of recrystallization. The bridging chloro-co-ligands affords a constrained 4-membered RuClRuCl ring with the opposing Cl1–Ru–Cl2 (84.94(2)°) bond angles being equal. In addition, an inversion of symmetry occurs about these chloro-co-ligands (*viz.* Cl1 and Cl2) and hence the geometrical parameters

around each metal centre is equivalent. Furthermore, the constrained 4-membered ring and bite angle (N2–Ru1–N1 = 87.93(7)°) induces non-linearity in the P1–Ru1–Cl2 (178.75(2)°), N2–Ru1–Cl1 (170.77(5)°) and N1–Ru1–Cl3 (175.55(5)°) bond angles.

The terminal Ru–Cl bonds (2.3744(7) Å) are significantly shorter than the bridging Ru–Cl bonds (Ru1–Cl1, Ru2–Cl2 = 2.4967(5) Å and Ru1–Cl2, Ru2–Cl1 = 2.4283(6) Å) and this trend is typical for chloro-bridged dinuclear ruthenium compounds. Intermolecular hydrogen-bonding is observed between the terminal chloro co-ligands and the amido hydrogen at 2.83(2) Å, see Fig. S20. The mononuclear complex **1** and dinuclear compound **4** share the same oxidation state and have comparable Ru–Cl (terminal for **4**) and Ru–P (2.3315(5) Å) bond lengths. The Ru–N$_{Schiff\ base}$ bond length of **4** (2.026(2) Å) is close to the lower limit of the 2.025(3)–2.151(4) Å range found for other ruthenium(III) compounds with Schiff base chelates [11,23,35–38]. In addition, the monoanionic charge donation of the amido nitrogen results in a shorter Ru–N$_{amido}$ (1.972(2) Å) bond of **4** in comparison to its Ru–N$_{Schiff\ base}$ bond. The tetrahydropyran (THP) moiety adopts a chair conformation which is common to many transition metal complexes containing chelators incorporating the THP core [39–43].

4. Conclusion

Novel ruthenium compounds bearing N, X-donor (X = O, N) heterocyclic chelators have been formed and spectroscopically characterized. X-ray analysis revealed that the metal atoms in the mono-(**1** and **2**) and dinuclear (**3** and **4**) metallic compounds are within centres of distorted octahedrons which are largely induced by the influence of chelating co-ligands. The crystal lattices of the respective complexes are stabilized by classical hydrogen bonding supported by weak intermolecular bonding which results in diverse supramolecular structures. A proposed formation route of compound **1** supported by the literature provided insight into the unique molecular transformation of Hbzap into the pho and bzca bidentate chelators. Furthermore, the redox properties of these metallic compounds are comparable to other ruthenium compounds found within the literature. In addition, the metallic compounds had significantly higher radical scavenging capabilities than their corresponding free-ligands and the natural antioxidant, Vitamin C.

Acknowledgements

Appendix A. Supplementary material

CCDC 1033047–1033049 contains the supplementary crystallographic data for this paper. These data can be obtained free of charge from The Cambridge Crystallographic Data Centre via www.ccdc.cam.ac.uk/data_request/cif. Supplementary figures S1–S20 associated with this article can be found, in the online version, at http://dx.doi.org/10.1016/j.ica.2015.04.031.

References

[1] J.B. Aitken, S. Antony, C.M. Weekley, B. Lai, L. Spiccia, H.H. Harris, Metallomics 1051 (2012) 4.
[2] S. Medici, M. Peana, V.M. Nurchi, J.I. Lachowicz, G. Crisponi, M.A. Zoroddua, Coord. Chem. Rev. (2014), http://dx.doi.org/10.1016/j.ccr.2014.08.002.
[3] G. Gupta, G. Sharma, B. Koch, S. Park, S.S. Lee, J. Kim, New J. Chem. 37 (2013) 2573.
[4] J. Novales, N. Jonkhoff, J.H. Acquaye, Polyhedron 62 (2013) 148.

[5] L. Oehninger, M. Stefanopoulou, H. Alborzinia, J. Schur, S. Ludewig, K. Namikawa, A. Muñoz-Castro, R.W. Köster, K. Baumann, S. Wölfl, W.S. Sheldrick, I. Ott, Dalton Trans. 42 (2013) 1657.
[6] M. Parveen, A.M. Malla, Z. Yaseen, A. Ali, M. Alam, J. Photochem. Photobiol., B 130 (2014) 179.
[7] Y. Li, Z. Yang, J. Wu, Eur. J. Med. Chem. 45 (2010) 5692.
[8] F. Arjmand, I. Yousuf, J. Organomet. Chem. 743 (2013) 55.
[9] B. Wang, Z. Yang, M. Lü, J. Hai, Q. Wang, Z. Chen, J. Organomet. Chem. 694 (2009) 4069.
[10] M. Morais, S. Subramanian, U. Pandey, G. Samuel, M. Venkatesh, M. Martins, S. Pereira, J.D. Correia, I. Santos, Mol. Pharm. 8 (2011) 609.
[11] I.N. Booysen, S. Maikoo, M.P. Akerman, B. Xulu, O.Q. Munro, J. Coord. Chem. 66 (2013) 3673.
[12] P. Krishnamoorthy, P. Sathyadevi, K. Senthilkumar, P. Thomas Muthiah, R. Ramesh, N. Dharmaraj, Inorg. Chem. Commun. 14 (2011) 1318.
[13] A.L. Spek, Acta Crystallogr., Sect. D65 (2009) 148.
[14] Bruker APEX2, SAINT and SADABS. Bruker AXS Inc. (2010) Madison, Wisconsin, USA.
[15] R.H. Blessing, Acta Crystallogr., Sect. A51 (1995) 33.
[16] G.M. Sheldrick, Acta Crystallogr., Sect. A64 (2008) 112.
[17] L.J. Farrugia, J. Appl. Crystallogr. 45 (2012) 849.
[18] N.G. Tsierkezos, A.I. Philippopoulos, Inorg. Chim. Acta 362 (2009) 3079.
[19] S.E. Diamond, F. Mares, B.S. Tovrog, 1980, US Patent 4207305A.
[20] Z. Dong, P.J. Scammels, J. Org. Chem. 72 (2007) 9881.
[21] F. Shia, M.K. Tsea, M. Beller, J. Mol. Catal. 270 (2007) 68.
[22] C.M. Che, W.P. Yip, W.Y. Yu, Chem. Asian J. 18 (2006) 453.
[23] I.N. Booysen, A. Abimbola, O.Q. Munro, B. Xulu, Polyhedron 73 (2014) 1.
[24] L. Bennett, J. Exp. Clin. Med. 4 (2012) 215.
[25] S. Li, G. Chen, C. Zhang, M. Wu, S. Wu, Q. Liu, Food science at Human Wellness, 2014, http://dx.doi/10.1016.fshw.2014.11.002.
[26] P. Ragendran, Clin. Chim. Acta 436 (2014) 332.
[27] T.S. Kamatchi, N. Chitrapriya, S.K. Kim, F.R. Fronczek, K. Natarajan, Eur. J. Med. Chem. 59 (2013) 253.
[28] T. Bal-Demirci, M. Şahin, E. Kondakçı, M. Özyürek, B. Ülküseven, R. Apak, Spectrochim. Acta, Part A 138 (2015) 866.
[29] Y.S. El-Sayed, M. Gaber, Spectrochim. Acta, Part A 137 (2015) 423.
[30] R. Ramachandran, P. Viswanathamurthi, Spectrochim. Acta, Part A 103 (2013) 53.
[31] G. Prakash, R. Manikandan, P. Viswanathamurthi, K. Velmurugan, R. Nandhakumar, J. Photochem. Photobiol., B 138 (2014) 63.
[32] P. Anitha, N. Chitrapriya, Y.J. Jang, P. Viswanathamurthi, J. Photochem. Photobiol., B 129 (2013) 17.
[33] J.G. Małecki, Polyhedron 31 (2012) 159.
[34] J.G. Małecki, A. Maron, Polyhedron 40 (2012) 125.
[35] R. Raveendran, S. Pal, J. Organomet. Chem. 692 (2007) 824.
[36] K. Nagaraja, S. Pal, J. Organomet. Chem. 745–746 (2013) 404.
[37] K. Nagaraja, S. Pal, J. Organomet. Chem. 737 (2013) 7.
[38] S. Mandal, V. Kundi, D.K. Seth, K. Srikanth, P. Gupta, Polyhedron 80 (2014) 290.
[39] D.T. Hill, B.M. Sutton, Cryst. Struct. Commun. 9 (1980) 679.
[40] P. Leibnitz, G. Reck, H.-J. Pietzsch, H. Spies, Forschungszent Rossendorf (ber) 311 (2001) 102.
[41] D. Schwidom, M. Volkmann, A. Wolter, J. Heck, Carbohydr. Res. 365 (2013) 26.
[42] M. Sternberg, J. Rust, C.W. Lehmann, F. Mohr, Helv. Chim. Acta 96 (2013) 280.
[43] Y. Mikata, Y. Sugai, M. Obata, M. Harada, S. Yano, Inorg. Chem. 45 (2006) 280.